Sebha University Journal of Pure & Applied Sciences Vol.25 No. 2 2026
DOI: 10.51984/pfk5wf62

مجلة جامعة سبها للعلوم البحتة والتطبيقية
Sebha University Journal of Pure & Applied Sciences

Journal homepage: www.sebhau.edu.ly/journal/jopas

Design and Aerodynamic Performance Evaluation of an Open-Circuit Subsonic Wind Tunnel Using Computational Fluid Dynamics

Abdallah Abuzrida

Department of Aeronautical Engineering, College of Civil Aviation, Misurata, Libya.

Keywords:
Computational Fluid Dynamics.
Contraction Cone Configurations.
Diffuser Configuration.
Pressure Recovery Coefficient.
Turbulent Intensity.
Aerodynamics Performance.

ABSTRACT

This study provides an assessment of the design and aerodynamic performance of an open-circuit subsonic wind tunnel using computational fluid dynamics. Eight wind tunnel configurations have been designed, combining two contraction geometries (curved and straight tapered), two diffuser angles (6 and 7 degrees), and two diffuser designs (conventional diffuser and square-to-circular transition diffuser). The aerodynamic performance of each model was evaluated by means of pressure distribution, speed distribution, turbulence intensity, and the pressure recovery coefficient. The results of the simulation showed that all configurations had successfully accelerated the airflow to a target speed of approximately 30 m/s in the test section. However, significant differences were observed in the performance of the diffuser and the quality of the downstream flow. Models incorporating a square-to-circle transition diffuser showed smoother pressure recovery, more uniform speed gradients, and significantly lower turbulence intensities than conventional diffuser models. These configurations also achieved higher pressure recovery coefficients (0.65-0.68), which suggests that dynamic pressure conversion is more efficient and that aerodynamic losses are reduced. Although model 2 had the highest-pressure recovery coefficient (0.72), it produced significantly more turbulence downstream of the diffuser. On the other hand, model 6, consisting of a curved deflector, a square-to-circular transition diffuser, and a 6-degree diffuser angle, provided the most balanced aerodynamic performance, combining high pressure recovery, stable speed distribution, and low turbulence. The findings show that optimization of both the contraction and diffuser geometry significantly improves the flow quality of the wind tunnel and provides practical design guidance for the development of efficient open-circuit subsonic wind tunnel aerodynamic testing at the laboratory scale.

تصميم وتقييم الأداء الديناميكي الهوائي لنفق رياح دون سرعة الصوت ذي دائرة مفتوحة باستخدام ديناميكيات الموائع الحسابية

عبدالله أبوزريدة

قسم هندسة الطيران، كلية الطيران المدني، مصراتة، ليبيا.

الكلمات المفتاحية:
ديناميكا الموائع الحسابية.
أشكال مخروط الإنقباض.
أشكال الناشر.
معامل استعادة الضغط.
شدة الاضطراب.
الأداء الديناميكي الهوائي.

الملخص

تقدم هذه الدراسة تقييمًا لتصميم وأداء الديناميكا الهوائية لنفق هوائي دون صوتي ذي دائرة مفتوحة باستخدام ديناميكا الموائع الحسابية. تم تصميم ثمانية نماذج لنفق هوائي، تجمع بين شكلين هندسيين للانقباض (منحني ومستقيم مدبب)، وزاويتين للناشر (6 و7 درجات)، وتصميمين للمشتت (مشتت تقليدي ومشتت انتقالي من المربع إلى الدائرة). تم تقييم الأداء الديناميكي الهوائي لكل نموذج من خلال توزيع الضغط، وتوزيع السرعة، وشدة الاضطراب، ومعامل استعادة الضغط. أظهرت نتائج المحاكاة أن جميع النماذج نجحت في تسريع تدفق الهواء إلى سرعة مستهدفة تبلغ حوالي 30 مترًا في الثانية في قسم الاختبار. ومع ذلك، لوحظت اختلافات كبيرة في أداء المشتت وجودة التدفق في اتجاه المصب. أظهرت النماذج التي

*Corresponding author.
E-mail addresses: abdullahabuzarida@misrataca.edu.ly.

Article History : Received 30 July 26 - Received in revised form 24 August 26 - Accepted 31 August 26

تتضمن مشتتًا انتقاليًا من المربع إلى الدائرة استعادة ضغط أكثر سلاسة، وتدرجات سرعة أكثر انتظامًا، وشدة اضطراب أقل بكثير من نماذج المشتت التقليدي. حققت هذه التكوينات أيضًا معاملات استعادة ضغط أعلى (0.68-0.65)، مما يشير إلى كفاءة أعلى في تحويل الضغط الديناميكي وانخفاض في الفقد الديناميكي الهوائي. على الرغم من أن النموذج 2 حقق أعلى معامل استعادة ضغط (0.72)، إلا أنه تسبب في اضطراب أكبر بكثير في اتجاه مجرى الهواء بعد المشتت. في المقابل، قدم النموذج 6، الذي يتكون من عاكس منحني، ومشتت انتقالي من الشكل المربع إلى الدائري، وزاوية مشتت 6 درجات، أداءً ديناميكيًا هوائيًا متوازنًا، جامعًا بين استعادة ضغط عالية، وتوزيع سرعة مستقر، واضطراب منخفض. تُظهر النتائج أن تحسين كل من هندسة الانقباض والمشتت يُحسّن بشكل كبير جودة تدفق الهواء في نفق الرياح، ويُوفر إرشادات تصميم عملية لتطوير اختبارات ديناميكية هوائية فعالة في نفق رياح دون سرعة الصوت ذي دائرة مفتوحة على نطاق المختبر.

1. Introduction

One type of device that can be used to regulate airflow is the wind tunnel. Creating a uniform airstream around the object of interest is the primary purpose of a standard wind tunnel. There is no justification for lowering the performance of a traditional wind tunnel because science and technology have advanced to the point where a safer and more precise wind tunnel design procedure is now possible [1]. After realizing that an object in airflow is comparable to an object moving in the air, Leonardo Da Vinci used the idea of a wind tunnel [2]. Francis Wenham built the first wind tunnel in history in Great Britain in 1871 [3]. Better designs were attempted to be implemented once scientists understood that reduced turbulence in the test section was essential. The wind tunnel is divided into two main groups: 1. Open circuit, 2. Closed circuit: Whereas the closed circuit offers many of the advantages mentioned in [4], there are also some disadvantages, such as pressure loss and loss of energy. Both open- and closed-circuit wind tunnels have certain similarities, such as the fact that it has an intake section, a contraction cone, a test section, a diffuser, and a fan for the airflow within the wind tunnel. Knowing its advantages, scientists have focused on several aspects to improve its performance, such as minimizing test section turbulence, laminar flow, and minimizing the minimum loss of pressure. One of the critical factors in designing a wind tunnel is its size, which depends in particular on the size of the contraction cone. This cone can be designed to accommodate an incoming flow by reducing its length and drastically changing its cross-section.

For low-speed applications (typically characterized by a Mach number below 0.4), subsonic wind tunnels are commonly categorized as either open-circuit (open-loop) or closed-circuit (closed-loop) systems [5]. In open-circuit tunnels, air is drawn from the surrounding environment, accelerated through the contraction and test section, and then discharged back to the laboratory or ambient space. This configuration is generally simpler, more compact, and less expensive to construct. However, it is more susceptible to environmental disturbances such as temperature variations, ambient turbulence, and acoustic reflections in the test room. Additionally, the discharged jet can create noise and flow interference if not properly managed [6]. Closed-circuit tunnels recirculate air within a ducted loop, reducing environmental interaction and often improving flow uniformity and stability, but at the cost of larger infrastructure, higher complexity, and greater capital expenditure [7]. For this reason, industrial aeroacoustics facilities frequently adopt closed-loop configurations to support stringent flow and noise requirements, whereas universities often select open-loop designs to reduce cost while pursuing acceptable performance through careful conditioning and measurement planning [8].

The contraction cone design is well illustrated in [9], where the 5th-order polynomial equation is recommended for the cross-sectional shape of the contraction cone and plays a key role in selecting the overall length of the contraction cone and wind tunnel. Although creating a cone-based polynomial on a cone is a daunting task, it is preferable because it greatly reduces the length of the contraction cone without separating the flow.

The purpose of the diffuser is to reduce the speed with as little energy loss as possible [10]. Obtaining good performance from the diffuser is critical to achieving high-quality flow in the test section, as incorrect dimensioning can cause intermittent or steady separation of the flow. A general rule of design of the diffuser is that the cone expansion shall not exceed 5 degrees of angle to ensure that the turbulent boundary layer is not separated. A low angle creates a larger pressure drop [11-12], suggesting that the diffuser should be positioned between 5° and 10° for optimal flow stability and pressure recovery. At angles slightly above 5°, the pressure recovery is increased, but this may result in the separation of the boundary layer and eventually unstable flow [13]. To minimize energy losses and recover static pressure, the diffuser is crucial. Overly large diffuser expansion angles can cause unfavorable pressure gradients, boundary-layer separation, and recirculation, all of which lower the wind tunnel's aerodynamic performance.

Because computational fluid dynamics (CFD) enables the rapid assessment of velocity distribution, pressure recovery, turbulence characteristics, and flow separation before fabrication, it has emerged as a successful method for optimizing wind tunnel geometry [14].

The design and operation of laboratory-scale subsonic wind tunnels have been studied recently; however, most of these studies have focused on a single contraction geometry or diffuser configuration. In a consistent CFD framework, a thorough comparison of the Bell-Mehta and straight-taper contractions for various diffuser angles and square-to-circular diffuser transitions is lacking.

The objective of this work is to design and study the aerodynamic performance of a subsonic wind tunnel using Computational Fluid Dynamics (CFD). Different contraction profiles and diffuser geometries were studied to investigate the effect on airflow characteristics and overall wind tunnel performance. The aerodynamic performance of each configuration was investigated using SolidWorks Flow Simulation (version 2022), which analyzed the velocity distribution, flow uniformity, pressure recovery, pressure drop, and flow separation. The results were used to identify the most effective wind tunnel configuration. This study excludes the fabrication and its reliance on simulation only.

2. Methodology: Wind Tunnel Design

The dimensions of the wind tunnel design rely on the available laboratory floor space. Based on this, the dimensions are determined. However, this study did not consider the available laboratory floor area and focused only on design and simulation. The design of the open wind tunnel is initially based on the dimensions of the test section, from which the dimensions of the other contacting parts are then designed. The dimensions of the test chamber are typically chosen based on the desired final tunnel length and also on the dimensions of the model to be tested within the test chamber.

The main components of the wind tunnel are the contraction, honeycomb, test section, and diffuser; therefore, the design process is focused on determining the appropriate dimensions of these components.

There are other components (auxiliary components) that have been designed in contact with the main components, such as a bell mouth entrance (air inlet); a settling chamber to prepare air to inlet to contraction by installing the honeycomb and screens inside it; and an exit chamber to install the proper fan to generate the airflow due to the pressure difference between the inlet and the outlet resulting from the

exit fan.
The following subtitles outline the design of each section of the wind tunnel.

a. Test section design

The test section is the main area for mounting and testing the aerodynamic model; therefore, its dimensions must correspond to the size of the model and the required flow characteristics. Before defining the length of the test section, the hydraulic diameter (D_H) of the test section pipe shall be calculated using the general formula in equation (1) [15].

$$D_H = \frac{4A_{T_S}}{P} \text{.................................... (1)}$$

Where P indicates the perimeter of the test section. To promote flow uniformity at the outlet and to reduce the probability of boundary layer separation at the outlet, the length of the test section (LT) is usually chosen to be between 0.5 to 3 times the hydraulic diameter, resulting in a length expression in equation (2) [16].

$$l_{T_s} = (0.5 - 3)D_H \text{ ....(2)}$$

The dimension of the test section is 300 mm × 300 mm, and the cross-sectional shape of the test section is square. The length of the test section is 600 mm.
Figure 1 illustrates the test section chamber design using SolidWorks.

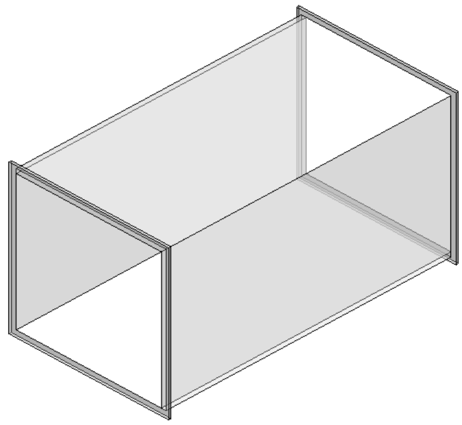

Figure 1: Test section chamber

b. The contraction cone design

For small-scale low-speed wind tunnels, the contraction ratio (CR) must be between 6 and 10, according to earlier research [4]. Furthermore, within that range, the test section's cross-sectional area must be less than 0.5 m², and the free stream's velocity must be less than 40 m/s [17]. Taking these factors into account, CR = 6 was selected. The overall performance of a tunnel is determined by design parameters such as length, wall profile, and Reynolds number [18]. However, separation of the flow occurs at the exit if the contraction length is too long. In the case of too short a contraction length, the boundary layer is separated near the outlet. The fifth-order polynomial curve meets most of the requirements by providing a minimum, and the separation of the flow occurs when the contraction length and the contraction intensity (Lc-Hi) exceed 0.667 to 1.79 [17].
The contraction ratio (CR) is represented in equation (3) as follows:

$$CR = \frac{A_{inlet}}{A_{outlet}} \text{ ....(3)}$$

Where A_{inlet} is the inlet cross-sectional area of contraction, and A_{outlet} is the outlet cross-sectional area of contraction, which is the inlet cross-sectional area of the test section chamber. The dimension of contraction is 735 mm × 735 mm, and the cross-sectional shape of the test section is square. The length of contraction is 588 mm.
In the contraction cone, the area of flow is decreased gradually, while the velocity of flow increases. In this study, there are two types of wall profiles of the contraction cone that were designed, which are: a straight slope profile (straight-taper contraction), and a polynomial fifth-order curved profile (Bell–Mehta contraction).
A fifth-order curved profile is represented in equation (4) as follows [9]:

$$r(x) = r_i + (r_o - r_i)\left[10\left(\frac{x}{L}\right)^3 - 15\left(\frac{x}{L}\right)^4 + 6\left(\frac{x}{L}\right)^5\right] \text{ ....(4)}$$

Where:
r_i: inlet half width = (735/2) = 367.5 mm.
r_o: outlet half width = (300/2) = 150 mm.
L: Contraction length = 588 mm.
x: distance from inlet (0 → L)
Figure 2 illustrates the wall profile of Bell-Mehta for the upper and lower surfaces of the contraction cone.

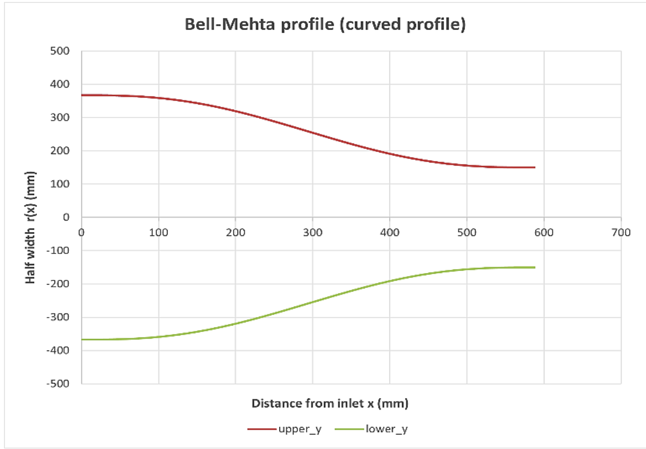

Figure 2: curved profile of contraction cone wall, Bell-Mehta profile

Figure 3 illustrates two selected types of contraction cones designed using SolidWorks; there is no change in the contraction cone ratio (CR) in this study.

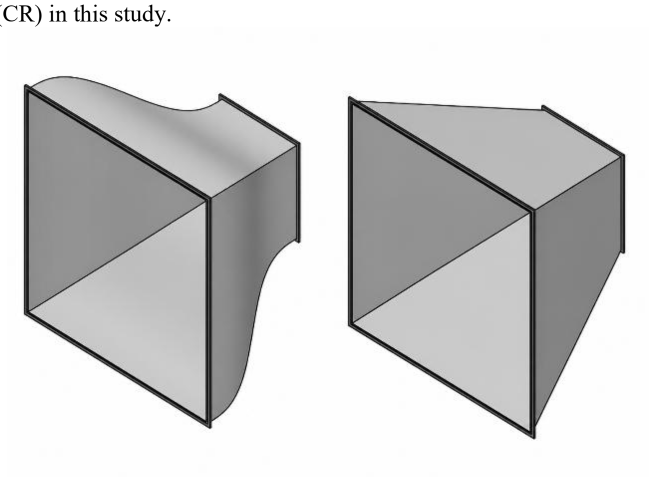

Figure 3: Curved (Bell-metha) and straight-taper contraction cone

c. Diffuser design

The diffuser is used downstream of the test section to slow the flow and restore static pressure as the cross-sectional area grows. Bernoulli-based relationships between velocity and pressure in internal flows are compatible with this behavior [19]. The diffuser and suction fan section is typically connected directly in open-circuit wind tunnels so that the diffuser exit area matches the suction inlet area [16]. The suction fan section-to-test-section area ratio (AR), which can be used to express the suction area section (A suction fan) as represented in equation (5) [5], is often set between two and three by practical design guidelines.

$$A_{suction-fan} = AR \,.\, A_{TS} \text{ ....(5)}$$

Where:
$A_{suction\text{-}fan}$: cross-sectional area of the suction fan section, which is the outlet cross-sectional area of the diffuser.
AR: area ratio between the diffuser outlet (suction fan) and the diffuser inlet, as represented in equation (6), as follows:

$$AR = \frac{A_{outlet}}{A_{inlet}} \text{ .... (6)}$$

A_{TS}: test section cross-sectional area.
In this study, the AR ratio was approximately 2.507; the outlet of the diffuser dimensions is 475 mm × 475 mm.
In order to minimize diffuser pressure losses, a half expansion angle (θe) of about 2°–4° is frequently used [20]. Consequently, equation (7) can be used to calculate the diffuser length (L_D).

$$L_D = r_1\left(\frac{\sqrt{AR}-1}{\tan\theta_e}\right) \text{ .... (7)}$$

Where:
L_D: length of diffuser.
r_1: half the length of the diffuser inlet height side.
θe: half expansion angle of the diffuser.

Four models were designed for the diffuser based on half-angle (θe), length, and outlet shape of the diffuser. The data of the models are tabulated in Table 1.

Table 1: Diffuser models parameters.

Diffuser models	Half-angle θe	Length (mm)	Inlet shape	Outlet shape
Model 1	3°	1670	Square	Square
Model 2	3.5°	1430.6	Square	Square
Model 3	3°	1670	Square	Circle
Model 4	3.5°	1430.6	Square	Circle

Figure 4 illustrates the four diffuser configurations designed using SolidWorks. There are two types of diffusers with two different expansion angles (6 and 7 degrees). The first is a square, and the second is a square-to-circle transition.

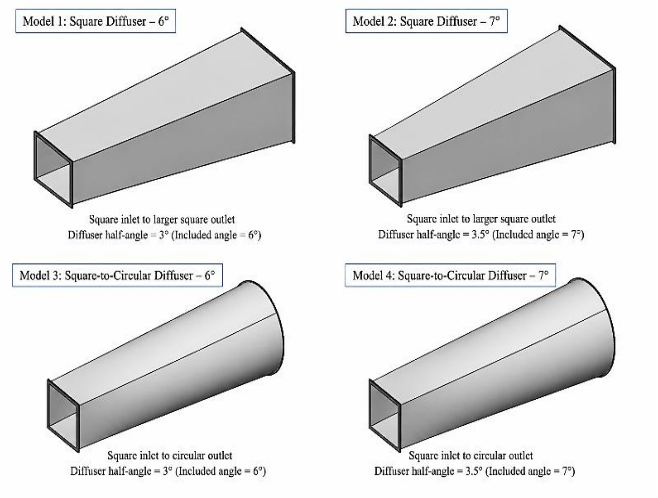

Figure 4: Diffuser configurations

d. Honeycomb design

In order to minimize pressure penalties and enhance a more linear, stable, and unidirectional inflow, the honeycomb (flow straightener) is placed upstream [21].

There are important factors to take into account when designing a honeycomb, such as the length (L_h), porosity (β_h), and cell hydraulic diameter (D_H). Porosity is defined as the exact flow area divided by the total cross-sectional area [9]. It is represented in an equation (8) as follows:

$$\beta_h = \frac{A_{flow}}{A_{total}} \quad (8)$$

The two primary requirements for honeycomb design are $6 \leq \frac{L_h}{D_H} \leq 8$ and $\beta_h \leq 0.8$. [9]. These requirements should be upheld for the best design conditions, and a settling chamber diameter of roughly 150 cells is thought to be practical.

In this study, the number of cells of the honeycomb is approximately 1156. The hydraulic diameter of each cell is 20 mm, and the length is 50 mm, so the L_h/D_H ratio of 2.5 is less than required, but it has an effect on real wind tunnel performance. In a simulation study, the inlet velocity is constant and uniform due to the design excluding the suction fan's effects. Figure 5 illustrates the honeycomb design using SolidWorks. The outlet frame dimension of the honeycomb is equal to the inlet dimension of the contraction cone and settling chamber. The honeycomb will be installed at the inlet of the settling chamber.

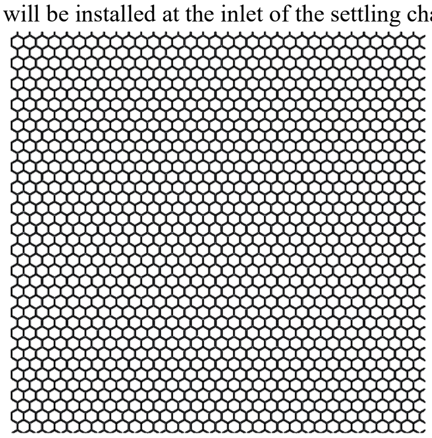

Figure 5: Honeycomb (airflow straightener)

e. Settling chamber

It is a chamber used to install the honeycomb (airflow straightener) and screens. Most of an open wind tunnel places it upstream of the contraction cone. In a real wind tunnel, the honeycomb is essential because it removes crossflow, reduces swirl, decreases large-scale turbulence, and improves velocity uniformity before the contraction.

In this study, the dimensions of the settling chamber are 735 mm × 735 mm × 400 mm. Figure 6 illustrates the setting chamber design using SolidWorks.

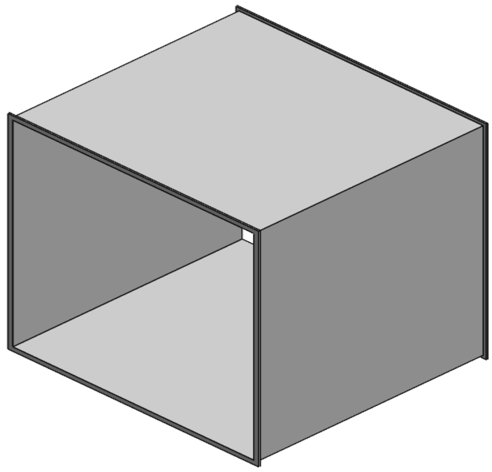

Figure 6: Settling chamber

f. Air inlet (air intake)

Most of the designed wind tunnels used this part to draw in as much air as possible. Mostly, the shape of the intake air, such as the bell mouth. In this study, the bell mouth has been simplified to a straight air inlet. The dimensions of the air inlet are 735 mm × 735 mm × 50 mm. Figure 7 illustrates the air inlet design in 3D using SolidWorks.

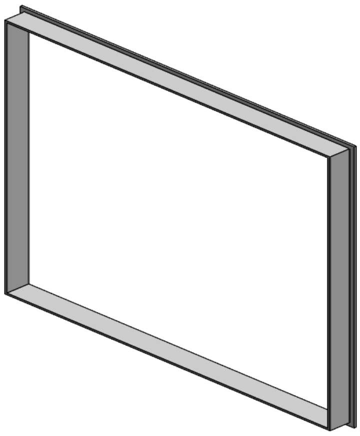

Figure 7: Air inlet (air intake)

g. Exit chamber (suction fan chamber)

In a real wind tunnel, the exit chamber (suction fan chamber) is used to install the suction fan. Some of the designs set the suction fan downstream after the diffuser directly. In this study, there is no suction fan used, and the airflow starts from the air inlet uniformly at 5 m/s. There are two designed models of the exit chamber based on the outlet shape of the diffuser, which are square and circular cross-sections. For the square-shaped model, the dimensions of the model are 475 mm × 475 mm × 400 mm, while for the circular-shaped model, the dimensions of the model are 475 mm in diameter and 400 mm in length. Figure 8 illustrates the two-exit chamber models that were designed using SolidWorks.

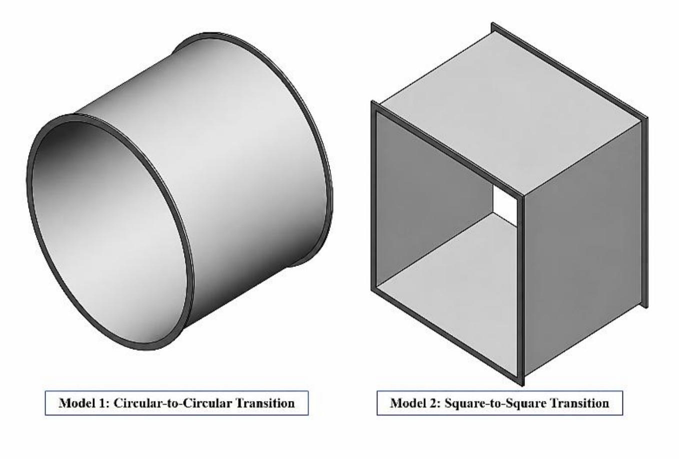

Figure 8: Exit chamber designed models

h. Assembly of wind tunnel components

In view of the fact that there were two proposed models of the contraction cone and four proposed models of the diffuser, eight wind tunnel models were designed for the purpose of evaluating aerodynamic performance. Table 2 illustrates the components of each model.

Table 2: Wind tunnel models components

Wind tunnel models	Contraction cone configurations	Diffuser configurations
Model 1	Bell-metha	Square - 7 degrees of expansion
Model 2	Bell-metha	Square - 6 degrees of expansion
Model 3	straight-taper	Square - 7 degrees of expansion
Model 4	straight-taper	Square - 6 degrees of expansion
Model 5	Bell-metha	Square to circle- 7 degrees of expansion
Model 6	Bell-metha	Square to circle- 6 degrees of expansion
Model 7	straight-taper	Square to circle- 7 degrees of expansion
Model 8	straight-taper	Square to circle- 6 degrees of expansion

Figure 9 illustrates the 3D wind tunnel assembly for model 1 using SolidWorks.

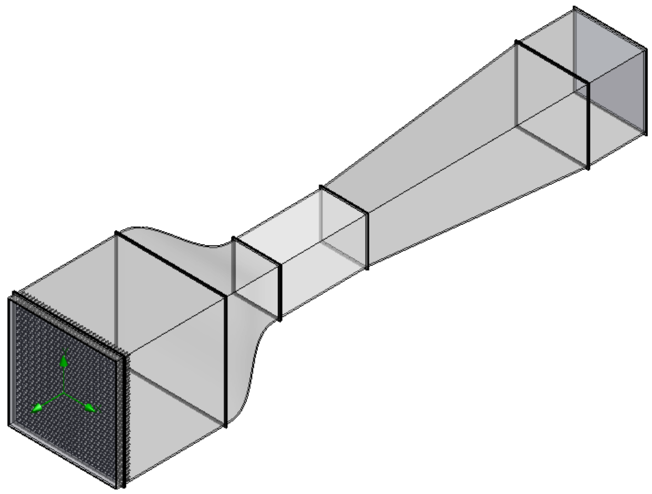

Figure 9: Wind tunnel assembly for model 1

3. Boundary Condition Parameters

The boundary conditions are essential for any simulation study. The air properties are important for airflow, such as the atmospheric air pressure, temperature, and density. The air inlet is set as an inlet of airflow at 5 m/s, and the exit chamber outlet face is set to be open to the atmosphere. Table 3 illustrates the boundary conditions conducted using the flow simulation.

Table 3: Boundary conditions parameters

Parameters	value	unit
Atmospheric pressure	101325	Pa
Temperature	288	K
Density	1.225	Kg/m^3
Inlet velocity	5	m/s
Outlet pressure	101325	Pa
Walls of the wind tunnel	adiabatic	--

4. Results and Discussion

The results will be divided into 3 parts, which are:

1- The pressure distribution contour through the wind tunnel.
2- The velocity distribution contour through the wind tunnel.
3- Comparison between the eight models designed based on pressure gradients, velocity gradient, turbulent intensity, and pressure recovery coefficient for the diffuser for each model.

All these results were conducted to evaluate the aerodynamic performance of each model.

a. The pressure distribution contour through the wind tunnel

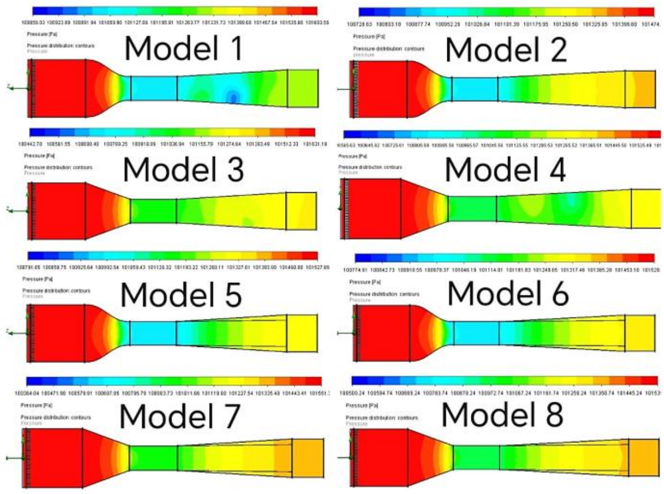

Figure 10: pressure distribution through the wind tunnel models

Figure 10 illustrates the pressure distribution through the wind tunnel models, as indicated by the results, which show that the static pressure of flowing air starts with a high value for all models, because the air velocity in this region is low. The static pressure begins to decrease gradually as the contraction cone is traversed. The lowest values of static pressure are at the entrance of the test section, where models 1, 2, 5, and 6 indicate the lowest static pressure in the test section region, and the rest of the models are moderate. In the diffuser region, models 1, 3, and 4 indicate vortices generated in the middle; these vortices will increase the turbulent intensity for these models, and the static pressure recovery for these models is the lowest compared with other models. Models 2, 5, 6, 7, and 8 indicate an acceptable static pressure recovery (increases gradually) through the diffuser; model 2 indicates the best model for static pressure recovery.

b. The velocity distribution contour through the wind tunnel

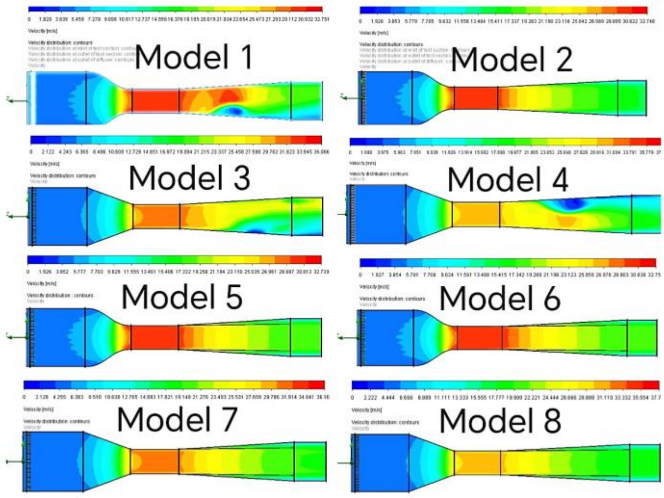

Figure 11: velocity distribution through the wind tunnel models

Figure 11 shows the velocity distribution contours for the eight wind tunnel models evaluated using computational fluid dynamics (CFD). In all models, airflow enters the settling chamber at a uniform, relatively low velocity, accelerates through the contraction section due to a decrease in cross-sectional area, reaches its maximum velocity in the test section, and then gradually slows in the diffuser. The results show that flow characteristics are heavily influenced by the geometry of the contraction and diffuser. Models with a curved contraction (Models 1, 2, 5, and 6) display smoother flow acceleration and more uniform velocity distribution in the test section than models with a straight tapering contraction (Models 3, 4, 7, and 8). This is because the curved design reduces unfavorable pressure gradients and boundary layer growth. Additionally, the Bell–Mehta contoured diffuser (Models 5–8) minimizes flow separation and offers a smoother velocity recovery compared to the conventional straight diffuser (Models 1–4). Models 5 and 6 show better aerodynamic performance, characterized by the most uniform velocity distribution and the least diffuser recirculation among all configurations. Conversely, Models 1 and 4 develop localized low-velocity zones and vortices at the diffuser outlet, indicating potential flow separation and decreased diffuser efficiency. Overall, the results confirm that combining a square-to-circle expansion diffuser with a curved contraction (Bell-Mehta) enhances flow uniformity, pressure recovery, and aerodynamic performance in the proposed open-circuit subsonic wind tunnel design.

c. Comparison between models

i. Pressure gradient through the wind tunnel

The static pressure distributions along the eight wind tunnel configurations are contrasted in Figure 12. In every model, there is a sharp pressure drop across the contraction section (Sections 4–5), where the airflow accelerates toward the test section, after the pressure in the settling chamber (Sections 1–4) stays largely constant. According to Bernoulli's principle, the increase in flow velocity causes the pressure to reach its lowest value within the test section (Sections 5–7). The static pressure gradually recovers as the airflow slows down as it enters the diffuser (Sections 8–11). There are discernible variations in the size of the pressure drop and the characteristics of the pressure recovery, even though all models show the same overall pressure trend. In addition to showing the highest flow acceleration, Model 2 also shows the lowest pressure in the test section and the largest pressure drop through the contraction, suggesting higher aerodynamic losses. Models 1, 5, 6, 7, and 8 show smooth and continuous pressure recovery within the diffuser along with moderate pressure reductions, indicating stable flow development and effective energy conversion. On the other hand, because of the straight contraction geometry, Models 3 and 4 maintain comparatively higher pressures throughout the test section, indicating lower flow acceleration. In comparison to the traditional straight diffuser (Models 1–4), the square to circle expansion diffuser (Models 5–8) typically offers smoother pressure recovery, indicating fewer unfavorable pressure gradients and less flow separation. Overall, the findings indicate that the most balanced aerodynamic performance can be obtained by combining a curved contraction with a Bell-Mehta contoured diffuser (especially Models 5 and 6), which achieves adequate pressure reduction in the contraction, maintains a stable low-pressure region in the test section, and provides effective pressure recovery in the diffuser.

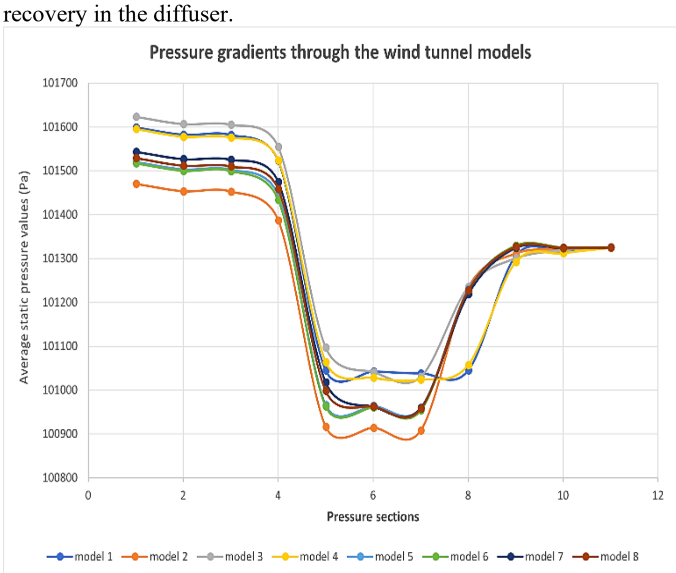

Figure 12: Comparison of pressure gradients through the wind tunnel models

ii. Velocity gradient through the wind tunnel

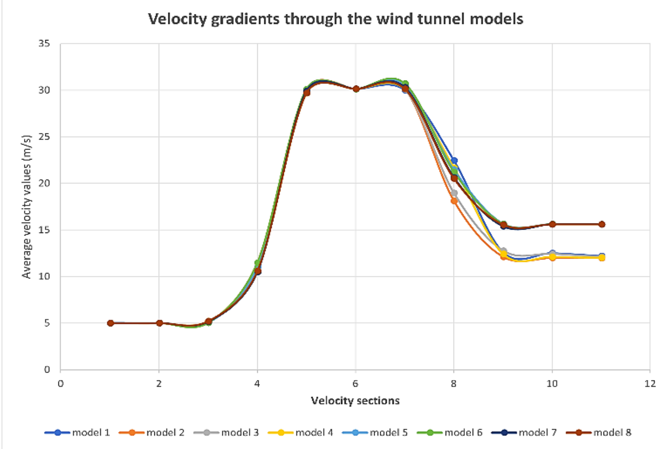

Figure 13: Comparison of the velocity gradient through the wind tunnel models

Figure 13 shows the velocity gradients over eight wind tunnel configurations derived from CFD simulations. The air enters the settling chamber at a nearly constant velocity of about 5 m/s, accelerates rapidly through the contraction section to a test pressure of approximately 30 to 31 m/s, and then slows in the diffuser as the flow expands towards the outlet. This velocity profile is common to all models. There are noticeable differences in the magnitude of acceleration and deceleration characteristics within the diffuser, although the overall acceleration trends are similar. Models 5 and 6, combining a square-to-circle expansion diffuser with a curved contraction (Bell-Metha), achieve the highest and most consistent speed in the test section—approximately 31 m/s—while maintaining a gradual and smooth reduction of the diffuser speed. This indicates a steady flow recovery, low energy loss, and efficient acceleration of the flow. Although models 7 and 8, which use a straight-line contraction with a square to circle expansion diffuser, also exhibit smooth speed recovery, their exit velocities are still relatively high, indicating less efficient conversion of kinetic energy to static pressure. Models 1-4, on the other hand, which have square-to-square expansion diffusers, see a more sudden drop in velocity following the test section. Models 2 and 4 have the lowest diffuser velocities among these, suggesting both greater pressure losses related to the diffuser geometry and stronger flow deceleration. Overall, the results show that the curved contraction improves flow acceleration and velocity uniformity prior to the test section, while the square-to-circle expansion diffuser offers a more controlled and stable velocity recovery than the traditional square-to-square expansion diffuser. The most advantageous aerodynamic performance is thus provided by the combination of a square-to-circle expansion diffuser (Models 5 and 6) and a curved contraction (Bell-Metha), which results in a highly uniform test-section velocity with smooth flow deceleration and decreased aerodynamic losses throughout the wind tunnel.

iii. Turbulent intensity through the wind tunnel

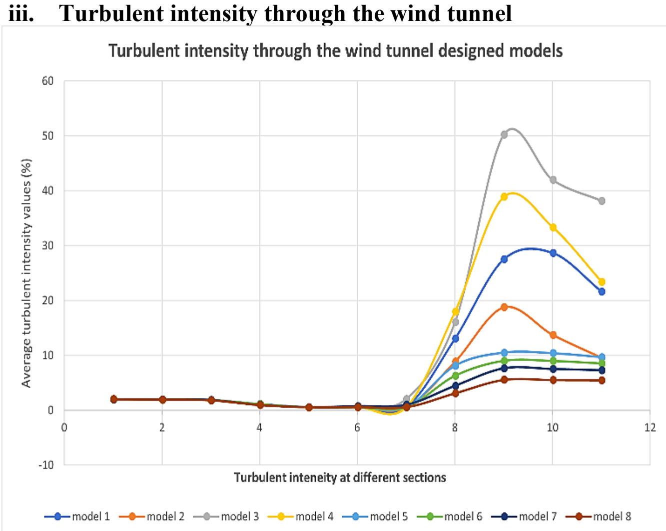

Figure 14: Comparison of the turbulent intensity through the wind tunnel models

The comparison of the turbulent intensity as shown in figure 14, for the eight wind tunnel models shows that the diffuser geometry plays an important role in the stability of the flow downstream of the test section, with the models that incorporate a straight (tapered) contraction cone (Models 3 and 4) having the highest turbulent intensity (50% and 39%, respectively) and a large degree of flow separation and recirculation in the diffuser, while the curved contraction cone (Bell-Mehta) (Models 1 and 2) produces a peak turbulent intensity of 29% and 19%, respectively, showing that a smooth contraction profile greatly reduces the flow disturbances, and the use of a square-to-circle transition diffuser (Models 5–8) further reduces the turbulent intensity due to the gradual cross-sectional transition, with Model 8 (straight (tapered) contraction cone plus square-to-circle transition diffuser) having the lowest turbulent intensity of about 10%. Models 6 and 7 also have relatively low turbulence levels (less than 10%), and Model 5 has a peak of around 10%, suggesting that a square-to-circle transition diffuser has better control over turbulence than a conventional straight diffuser, although the diffuser angle also plays a role. Model 8 has the best aerodynamic performance with the lowest turbulent intensity, which would indicate the best flow uniformity and least energy loss, so it would be the most suitable configuration for subsonic wind tunnel applications.

iv. Pressure recovery coefficient of the diffuser for each model

The pressure recovery coefficient (Cp) gauges a diffuser's effectiveness in converting airflow's kinetic energy into static pressure. Increased aerodynamic efficiency and decreased flow separation are the results of the diffuser recovering a greater percentage of the dynamic pressure with lower energy losses when the pressure recovery coefficient is higher. The following is the expression for the pressure recovery coefficient as shown in equation (9).

$$C_p = \frac{P_{out} - P_{in}}{\frac{1}{2}\rho V_{in}^2} \quad \text{……………………………..(9)}$$

Where:

P_{in}: the static pressure at the diffuser inlet (pa),

P_{out}: the static pressure at the diffuser outlet (pa),

ρ: air density (kg/m^3), and

V_{in}: average velocity at the diffuser inlet (m/s).

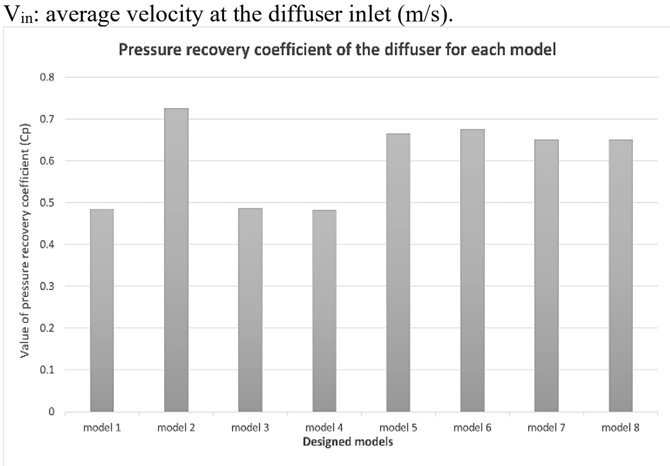

Figure 15: Comparison of the pressure recovery coefficient between 8 designed models

Figure 15 shows the pressure recovery coefficient for the eight wind tunnel models. The data clearly show that the diffuser geometry is critical to pressure recovery performance, and models 1, 3, and 4, with a straight diffuser, have the lowest pressure recovery coefficients (about 0.48), which shows that the conventional straight diffuser offers little pressure recovery because of higher pressure losses and a higher chance of flow separation. By contrast, model 2, which is a combination of a curved contraction cone and a 6° straight diffuser, has the highest-pressure recovery coefficient (about 0.73), which shows that it can convert dynamic pressure into static pressure most effectively. The models with a square-to-circle transition diffuser (models 5–8) also have high pressure recovery coefficients ranging from about 0.65 to 0.68, and higher than the straight diffuser configurations, with Model 6 (curved contraction with a square-to-circle transition diffuser and a 6° diffuser angle) having the highest-pressure recovery of about 0.68 and Models 5, 7, and 8 having nearly identical values of about 0.65–0.66. These results indicate that the gradual geometric transition from a square test section to a circular outlet improves pressure recovery by creating more gradual flow diffusion with lower adverse pressure gradients. Overall, Model 2 still has a higher turbulent intensity than models 6–8, despite having the highest-pressure recovery coefficient. Therefore, the square-to-circle transition diffuser configurations, especially Model 8, offer a more balanced aerodynamic performance and are better suited for subsonic open-circuit wind tunnel applications when pressure recovery, velocity uniformity, and turbulence characteristics are taken into account.

5. Conclusion

In order to examine the effects of contraction geometry, diffuser configuration, and diffuser angle on aerodynamic performance, this study successfully designed and assessed eight open-circuit subsonic wind tunnel configurations using Computational Fluid Dynamics (CFD). The test-section velocity of about 30 m/s was achieved by all models, according to the results; however, there were notable variations in pressure recovery, velocity uniformity, and turbulent intensity. Compared to models with traditional straight diffusers, models using the square-to-circle transition diffuser showed significantly reduced turbulent intensity, more stable velocity distributions, and smoother pressure recovery. Additionally, these models showed higher pressure recovery coefficients (roughly 0.65–0.68), suggesting lower aerodynamic losses and more effective pressure recovery. Model 6, which combines a curved contraction with a square-to-circle transition diffuser and a 6° diffuser angle, outperformed the other eight configurations in terms of overall aerodynamic performance. It achieved the lowest turbulence levels, uniform velocity distribution, and high-pressure recovery. These results show that careful optimization of the contraction and diffuser geometries can greatly enhance the flow quality of wind tunnels and offer helpful design guidance for the creation of effective open-circuit subsonic wind tunnels at the laboratory scale.

6. References

[1] M. M. Rahman, I. Bhuiyan, M. H. Ali, M. A. Islam, and S. Paul, “Design, fabrication and performance analysis of a subsonic open-circuit wind tunnel,” in Proceedings of the 7th International Conference on Mechanical, Industrial and Energy Engineering (ICMIEE 2022), Khulna, Bangladesh, Dec. 22–24, 2022, Paper ID: 187.

[2] D. D. Baals and W. R. Corliss, “Whirling arms and the first wind tunnels,” NASA Glenn Research Center. [Online]. Available: https://www.grc.nasa.gov/WWW/K-12/WindTunnel/history.html. [Accessed: Jul. 21, 2026].

[3] P. Bradshaw and R. C. Pankhurst, “The design of low-speed wind tunnels,” Progress in Aerospace Sciences, vol. 5, pp. 1–69, 1964, doi: 10.1016/0376-0421(64)90003-X.

[4] M. A. González Hernández, A. I. Moreno López, A. A. Jarzabek, J. M. Perales Perales, Y. Wu, and S. Xiaoxiao, “Design methodology for a quick and low-cost wind tunnel,” in Wind Tunnel Designs and Their Diverse Engineering Applications, IntechOpen, 2013, doi: 10.5772/54169.

[5] J. B. Barlow, W. H. Rae, and A. Pope, Low-Speed Wind Tunnel Testing, 3rd ed. New York, NY, USA: John Wiley & Sons, 1999.

[6] E. Rubino and T. Ioppolo, “Design, fabrication and performances of a closed-circuit subsonic wind tunnel,” in 55th AIAA Aerospace Sciences Meeting, AIAA SciTech Forum, Grapevine, TX, USA, 2017, doi: 10.2514/6.2017-0105.

[7] J. D. Pereira, Wind Tunnels: Aerodynamics, Models, and Experiments. New York, NY, USA: Nova Science Publishers, 2011.

[8] M. Pott-Pollenske, W. von Heesen, and A. Bergmann, “Acoustical preexamination work and characterization of the low noise wind tunnel DNW-NWB,” in 18th AIAA/CEAS Aeroacoustics Conference (33rd AIAA Aeroacoustics Conference), Colorado Springs, CO, USA, Jun. 4–6, 2012, AIAA-2012-2175, doi: 10.2514/6.2012-2175.

[9] R. D. Mehta and P. Bradshaw, “Design rules for small low-speed wind tunnels,” The Aeronautical Journal, vol. 83, no. 827, pp. 443–449, 1979, doi: 10.1017/S0001924000031985.

[10] M. M. Fouad, A. A. Hassan, and H. M. El-Batsh, “Design and construction of an open loop subsonic high temperature wind tunnel for investigation of SCR dosing systems,” International Journal of Thermofluids, vol. 11, Art. no. 100106, 2021, doi: 10.1016/j.ijft.2021.100106.

[11] J. M. Robertson and H. R. Fraser, “Separation prediction for conical diffusers,” Journal of Basic Engineering, vol. 82, pp. 201–209, 1960.

[12] R. D. Mehta, “The aerodynamic design of blower tunnels with wide-angle diffusers,” Progress in Aerospace Sciences, vol. 18, pp. 59–120, 1979, doi: 10.1016/0376-0421(77)90003-3.

[13] R. D. Mehta, “The aerodynamic design of blower tunnels with wide-angle diffusers,” Progress in Aerospace Sciences, vol. 18, pp. 59–120, 1979, doi: 10.1016/0376-0421(77)90003-3.

[14] D. L. Jayasooriya, C. V. P. Wedikkara, H. K. H. Kodithuwakku, and N. Samaraweera, “A design framework for subsonic low-speed wind tunnels,” in 2023 Moratuwa Engineering Research Conference (MERCon), Moratuwa, Sri Lanka, 2023, pp. 161–166, doi: 10.1109/MERCon60487.2023.10355478.

[15] Y. A. Çengel and J. M. Cimbala, Fluid Mechanics: Fundamentals and Applications, 3rd ed. New York, NY, USA: McGraw-Hill, 2014.

[16] S. Mauro, S. Brusca, R. Lanzafame, F. Famoso, A. Galvagno, and M. Messina, “Small-scale open-circuit wind tunnel: Design criteria, construction and calibration,” International Journal of Applied Engineering Research, vol. 12, no. 23, pp. 13649–13662, 2017.

[17] J. H. Bell and R. D. Mehta, Contraction Design for Small Low-Speed Wind Tunnels, NASA Contractor Report NASA-CR-182747, JIAA Technical Report 84. Stanford, CA, USA: Stanford University, Joint Institute for Aeronautics and Acoustics, 1988.

[18] T. Morel, “Comprehensive design of axisymmetric wind tunnel contractions,” Journal of Fluids Engineering, vol. 97, no. 2, pp. 225–233, 1975, doi: 10.1115/1.3447255.

[19] K. Yanel and A. Yanto, “Design of low subsonic wind tunnel with open return system for testing wind turbines at low airspeeds,” SINTEK JURNAL: Jurnal Ilmiah Teknik Mesin, vol. 17, no. 2, pp. 82–96, 2023, doi: 10.24853/sintek.17.2.82-96.

[20] R. van Dommelen, Design of an Atmospheric Boundary Layer Wind Tunnel, M.Sc. thesis, Eindhoven University of Technology, Eindhoven, The Netherlands, 2013.

[21] A. A. Wicaksana, R. Wibowo, and M. Kabib, “Analisa intensitas turbulensi aliran udara pada honeycomb dengan bentuk penampang melingkar untuk wind tunnel subsonic,” Jurnal Crankshaft, vol. 3, no. 1, pp. 19–24, 2020, doi: 10.24176/crankshaft.v3i1.4624.